

So Many Needles, So Little Time: Modeling Microneedle Injection of Anesthetics Into Human Skin

BEE 4530: Computer Aided Engineering – Applications to Biomedical Processes

Group #3:
Revanth Baddam
Stefan Engst
Randall Meyer
Archana Rachakonda

Table of Contents

1. Executive Summary -----	2
2. Introduction -----	3
3. Design Objectives -----	4
4. Results and Discussion -----	5
5. Conclusion and Design Recommendations -----	13
6. Appendix A: Mathematical Statement of the Problem -----	14
7. Appendix B: Solution Strategy -----	19
8. References -----	24

1. Executive Summary

Microneedles are a safe, simple to use, and painless alternative to common practices in local anesthesia. Although there have been many successful clinical trials utilizing this technology, there exists a need to optimize these devices for wide scale production and distribution. While several published models consider only one needle, there exists no simulation that realistically considers the effect of an array of needles in three dimensional tissue deliveries for optimization. In order to determine the ideal parameters for an experimental study (number of needles, spacing, etc.), a computer model was generated to simulate the injection and diffusion process into the skin.

The replica was completed in COMSOL to simulate a variable number of needles injecting anesthetic into a slab of human skin over the course of 1 minute. Convection, diffusion and fluid flow were incorporated utilizing simultaneous implementation of the mass transport and weakly compressible Navier-Stokes equations. Upon completion of this model, parameters including initial anesthetic concentration in the needles, number of needles and spacing of needles were varied to determine their effect on time to complete anesthesia of the dermis layer.

Results imply the initial concentration of anesthetic in the needles resulted in a significant increase in successful drug delivery. Therefore, this parameter is important in microneedle design. In terms of the number of needles and spacing, it was found that the optimal number was 25 needles spaced 500 μm apart. Although a limited number of possibilities were tested, this indicates a trend that for targeted local anesthesia, there is an optimal design in compact spacing.

Utilization of this computer model has allowed for the quick, inexpensive optimization of the microneedle drug delivery process. With the optimized parameters derived from this simulation, the device can be mass produced. This will allow medical practitioners and patients to reap all of the benefits of this technology, including its safety, ease of use, and painless drug delivery mechanism.

2. Introduction

Local anesthesia refers to the temporary induction of sensory loss in a localized area of the body. The ideal system of anesthesia should have a rapid effect upon administration, cause minimal pain, be safe to implement, and require minimal training. Typical procedures for the administration of local anesthetics involve multiple injections of compounds into the subcutaneous, intramuscular, or intradermal space at the intended site of surgery. Such protocols involve the use of hypodermic needles. Although effective in the delivery of compounds, these devices have several disadvantages. First and foremost is the patient's experience of pain from penetration of the nerve layer in the dermis due to the size of the needle. Such pain can generally create a sense of distress and anxiety, especially in children [1]. Another concern in the use of large hypodermic needles is safety. Sharps injuries are prevalent in both undeveloped countries and across healthcare workers in the U.S. numbering as high as 0.18 injuries/healthcare worker in 2003 [2]. These incidents can result in the spread of infectious agents such as HIV and hepatitis C and warrants the need to develop safer alternatives to current protocols. Finally, the use of hypodermic needles requires medical training that could be circumvented by a hypodermal injection-free alternative [3].

Recently, several needle-free alternatives have been developed. One of these is the use of topical anesthetic creams. This technique allows for the onset of drug delivery without the pain or the safety concerns associated with a physical injection. However, because this method relies completely on passive diffusion through the epidermis, the onset of anesthesia can occur up to 1.5 hours post administration [4]. Another alternative in commercial use is a disposable-cartridge jet injector, which involves the use of high, concentrated pressure to penetrate the epidermis and deliver a compound. These devices have been successfully implemented in mass scale vaccinations due to their ease of use. However, they break the skin barrier giving rise to the potential for disease transmission. In addition, there are alternative technologies such as laser/thermal ablation, ultrasonic-based techniques, and iontophoresis which have been created to address the desire for a needle free delivery system. Although used in the past, there has been poor market reception to these alternatives and their use has become discontinued in many developed countries [5].

The most promising and popular area of research surrounding the needle-free delivery of anesthetics involves the use of microneedles. Microneedles are minimally invasive in that they cause no sensation of pain due to their small size and penetration depth of no more than 100 microns into the skin. In addition, these delivery devices are easily fabricated in mass quantities, are as simple to use as a patch or cream, and preserve the rapid onset action of the pressure driven flow in a macro-scale hypodermic needle. Microneedles have been recently developed and utilized in numerous clinical tests, including the administration of influenza vaccines [6] and the regular injection of insulin [7]. In addition, microneedle administration of anesthetics has been utilized to administer anesthetics with an efficacy evaluated to be identical to one injection of a hypodermic needle [5].

Despite the success microneedle devices have had recently in clinical trials, there exists a need to optimize the design for mass production. Experimentation with different sized arrays of microneedles confirms the efficacy of the device, but does not ensure that it is operating at maximal capacity. To prepare for a large experimental study which would require potentially hundreds of devices to different specifications and equally as many clinical trials, a computer model of the microneedle injection process should be created. Numerous simulations of the local anesthetic procedures could then be run without the cost associated with clinical trials.

Model development for the microneedle injection process has thus far been limited to mimic the fluid flow of anesthetic in one needle. A computational model was developed by Lhernould and Delchambre to optimize the specifications of a single needle based on the pressure response and velocity field through a simulated tissue [8]. In addition, an analytical model was developed utilizing multiple flow rate measurements for the injection of one needle into chicken skin [9]. However, it was noted by the authors that extensive research would be required before the exact nature of the fluid mechanics through the tissue could be understood. To date, there is no computational or analytical model that considers the effect of multiple needles that can be used to answer the critical questions surrounding the microneedle injection process. These questions include the sensitivity of the concentration of anesthetic administered to the time of anesthesia and the effect of needle spacing and number on efficacy of drug delivery. In this study, we developed a computer simulation in COMSOL that can be utilized to study these aspects of microneedle drug delivery. Such a model can be utilized to optimize this injection technology for mass production and implementation on a global scale.

3. Design Objectives

There were three design objectives for this project:

- Develop a simplified 2-D model of microneedle injection to study aspects of a single microneedle injection and a complex 3-D model to simulate arrays of microneedle injection devices simultaneous into the skin layer.
- Determine the sensitivity of initial concentration of anesthetic in the microneedle to rate of delivery.
- Validate the model for optimization studies of microneedle injection with respect to number of needles in the array and their respective spacing.

4. Results and Discussion

2-D Simplified Solution

The model for the 2-D solution was developed as given by the procedures in Appendix A and Appendix B.

Given the mesh convergence, the solution at the end of 60 seconds was considered validated with respect to the discretization of the domain (Figure 1).

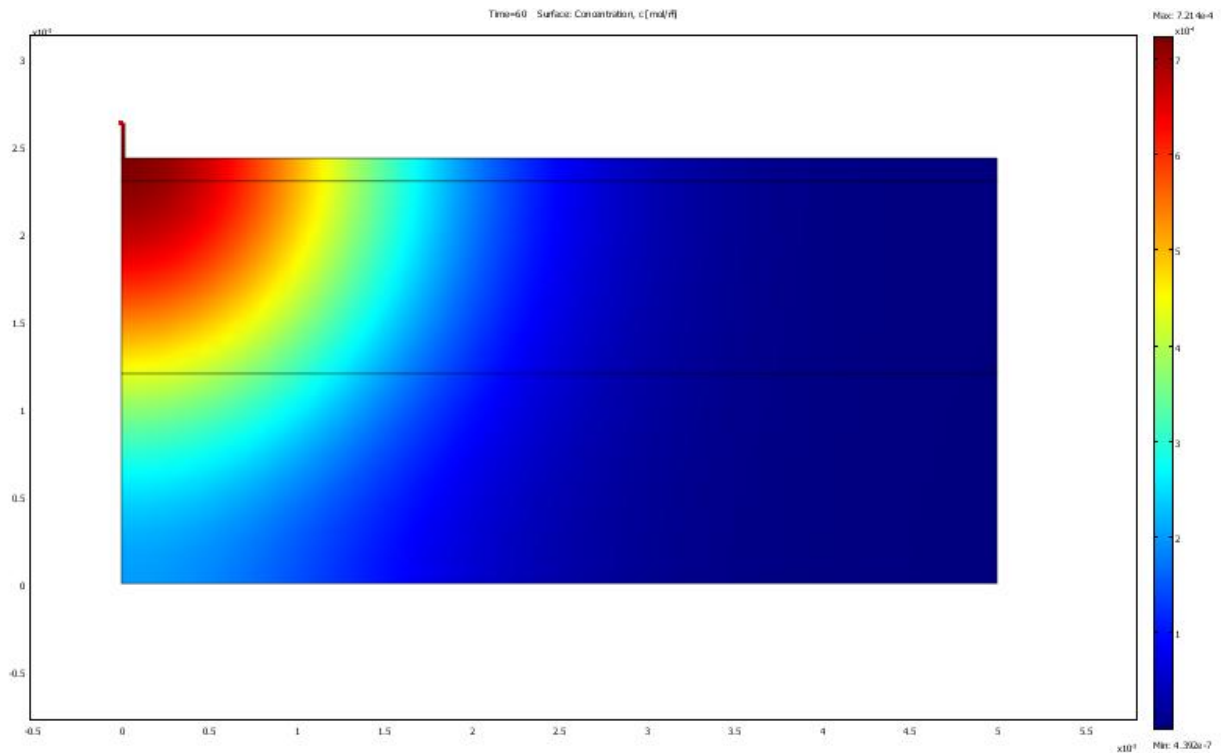


Figure 1: Concentration of lidocaine in the 2D model after 60 seconds. The model, as expected, shows that the concentration is the highest at the needle and slow drops as the distance from the microneedle increases.

The concentration profile of the anesthetic demonstrated a radially decreasing amount of drug delivery originating from the insertion point of the needle. This suggests that the primary mechanism for drug dispersion is diffusion, as opposed to the downward fluid flow imposed by the pressure in the needle.

The concentration vs. time profile of the drug taken at the same point as the mesh convergence was used to evaluate the drug delivery efficiency of one needle (Figure 2).

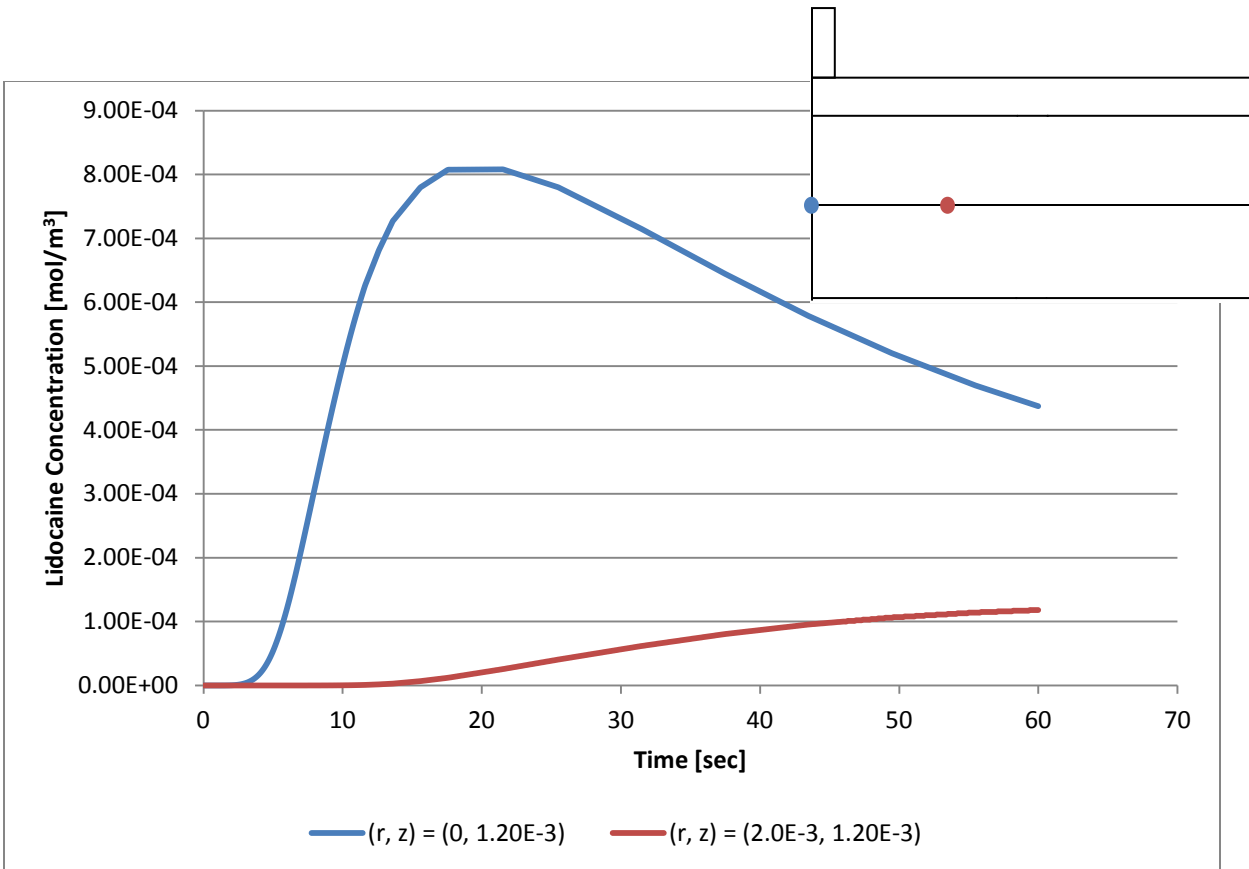


Figure 2: Concentration of lidocaine in the 2D model at two different points. At the point $(r, z) = (0, 1.20e-3)$, which is located directly under the needle at the nerve layer, the concentration reaches a maximum at around 0.0008 mol/m^3 within the first 20 seconds and drops for the rest of the time. As the concentration needed at the nerve layer is 0.004267 mol/m^3 , this concentration is lower than the concentration required for lidocaine to be effective. The point $(r, z) = (2.0e-3, 1.20e-3)$ is located at the dermis-fat layer interface farther away from the needle injection site. There is an increase in lidocaine concentration within the one minute time step, yet over the given time period, the concentration does not reach a maximum. The 2D schematic in the top right corner denotes the position of the two points.

Based on this plot, the drug concentration reached a maximum value as the compound was quickly transported to the interface due to high concentration gradients, but then began to diffuse away slowly as time progressed to the end of the model. The concentration achieved by one needle injection was also insufficient to achieve anesthesia of the region, reaching a maximum value of $9 \times 10^{-4} \text{ mol/m}^3$ and then progressing to a lower steady state value. The concentration vs. time profile was also evaluated farther away from the injection site at the point of $(r = 2.0e-3, z = 1.2e-3)$. The concentration of drug increased over the time of the model indicating the drug was being transported to this location. However, the amount that was transported ($\sim 1.0 \times 10^{-4} \text{ mol/m}^3$) was insignificant compared to the amount that was delivered right below the needle. The diffusion of the anesthetic from the needle can therefore be considered localized to the point of application.

3-D Complex Solution

The 3-D model of the anesthetic injection was developed according to the procedures detailed in Appendix A and Appendix B.

Given the results of the mesh convergence studies, the solution was considered validated with respect to discretization error. The concentration profile at $t = 60$ s, shown in Figure 3 reveals a similar trend in in the 3-D solution as it did in the 2-D solution, shown in Figure 2.

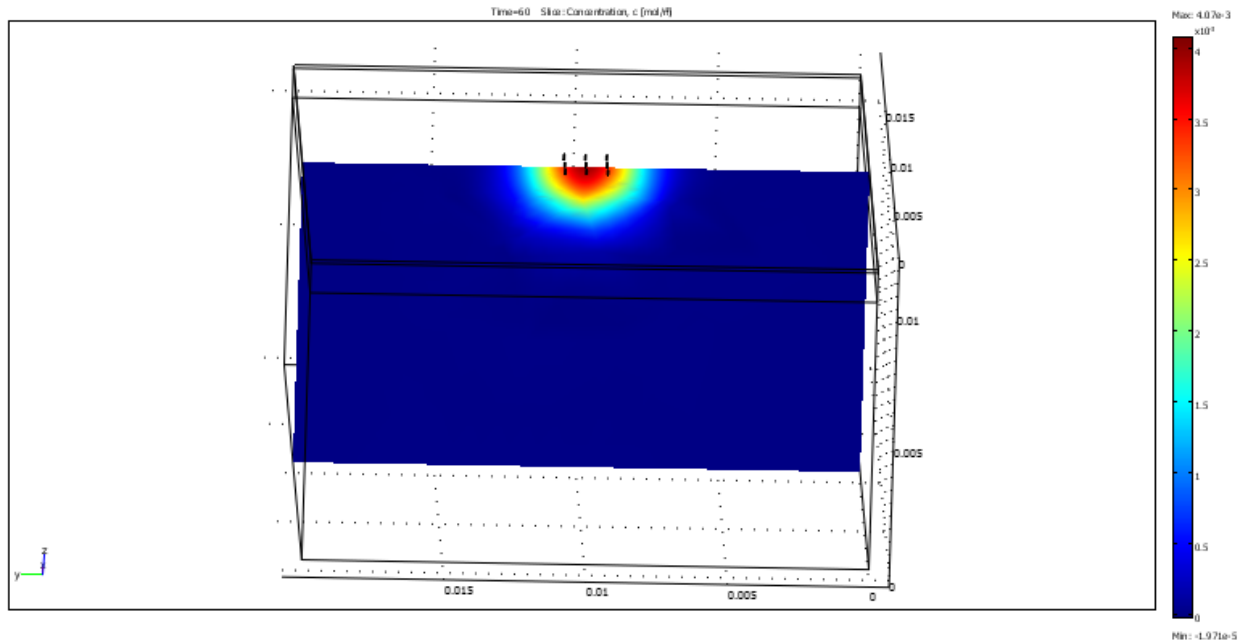


Figure 3: The concentration profile of lidocaine in the skin at one minute. The pattern indicates that the transport of the drug is mainly via diffusive flux, since the concentration drops in a radially symmetric manner originating at the point of needle injection.

There is a radially symmetric drop in concentration of the anesthetic originating from the point of injection signifying that diffusion is the critical mechanism to drug delivery in this case. With 9 needles, as designed in the original mesh, the concentration is still insufficient to induce local anesthesia at the dermis-fat layer interface (reaching a maximum of $4 \times 10^{-3} \text{ mol/m}^3$ in this region).

Sensitivity Analysis:

Upon successful computation of the solution, it was necessary to determine which parameters are important in drug delivery, as well as the impact of error in these estimated values. To accomplish this task, a sensitivity analysis was conducted on the model with respect to permeability, diffusivity, and initial concentration of anesthetic in the needles, as shown in Figure 4.

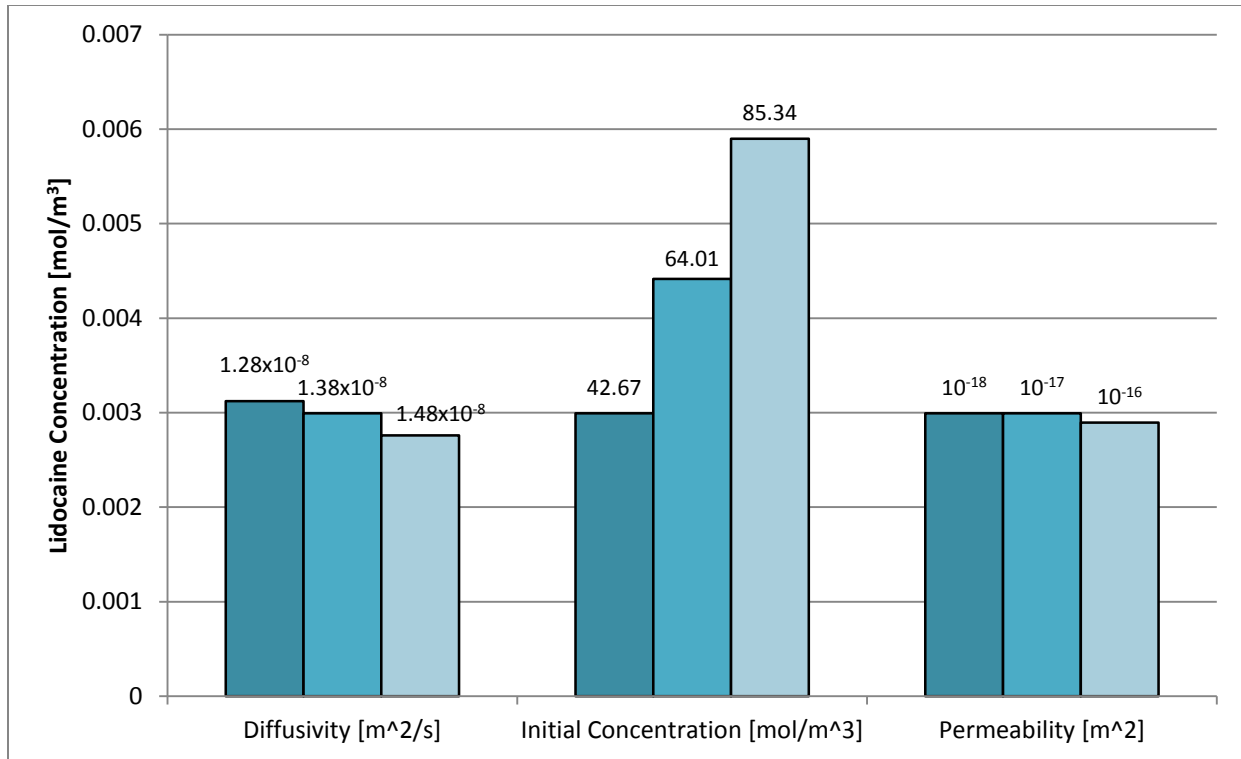


Figure 4: Sensitivity analysis for 3D model. The lidocaine concentration at point $(x, y, z) = (0.01, 0.01, 0.01)$ after 60 seconds was measured for a range of parameter values (diffusivity, initial lidocaine concentration in the microneedles, permeability).

The analysis was performed at the point $(x, y, z) = (0.01, 0.01, 0.01)$, similar to the mesh convergence, as the point was located at the center of the interface between the dermis and fat layers where we approximated the location of the nerves. The effect of variation in parameter values as a range on the concentration of lidocaine at the point was observed. Concentration values were taken at time $t = 60$ seconds. The value ranges chosen were based on error ranges reported in the parameter source material.

The model is most sensitive to changes in initial concentration of lidocaine in the microneedles. The model assumed an initial concentration of 42.67 mol/m^3 in the needles. To test the sensitivity of the model, the program was run again at 64.01 mol/m^3 and 85.34 mol/m^3 . As expected, the concentration at time $t = 60$ sec increased with increase in initial concentration. As more lidocaine is present in the needles prior to application of the patch, there will be more lidocaine observed in the skin after the same time frame.

The model is also sensitive to diffusivity of the drug in skin, although it does not vary as significantly. The current model assumes a diffusivity value of $1.38 \times 10^{-8} \text{ m}^2/\text{s}$. To test the sensitivity of the model, the program was run at a lower and higher diffusivity value than the one mentioned ($1.28 \times 10^{-8} \text{ m}^2/\text{s}$ and $1.48 \times 10^{-8} \text{ m}^2/\text{s}$). At a higher diffusivity value, the lidocaine concentration observed at the point was less than the current model while the opposite occurred for the lower diffusivity value. This is expected since with a higher diffusivity value, lidocaine travels faster through the skin layers, and thus after the same time frame of 60 seconds, less lidocaine would be seen at the point.

The model is least sensitive to permeability of the skin. Running the program at a range of permeability values from 10^{-16} m^2 to 10^{-18} m^2 had small to negligible change in lidocaine concentration. To account for the change in porosity of the skin with permeability, the porosity value was scaled with permeability according to their related equation, stated in Appendix A. Similar to diffusivity, at the highest permeability value, the lidocaine concentration was less than that of the current model. The influence of permeability on fluid flow is not significant in comparison to the influence of diffusion in the movement of lidocaine through skin, validating the qualitative results previously determined (Figure 1 and Figure 3).

Optimization:

The last part of the study was devoted to demonstrate usage of the model for optimization studies regarding the number of needles, their spacing, as well as the initial concentration of anesthetic in the needle. The relationship between number of needles and the initial concentration of anesthetic was considered first in Figure 5.

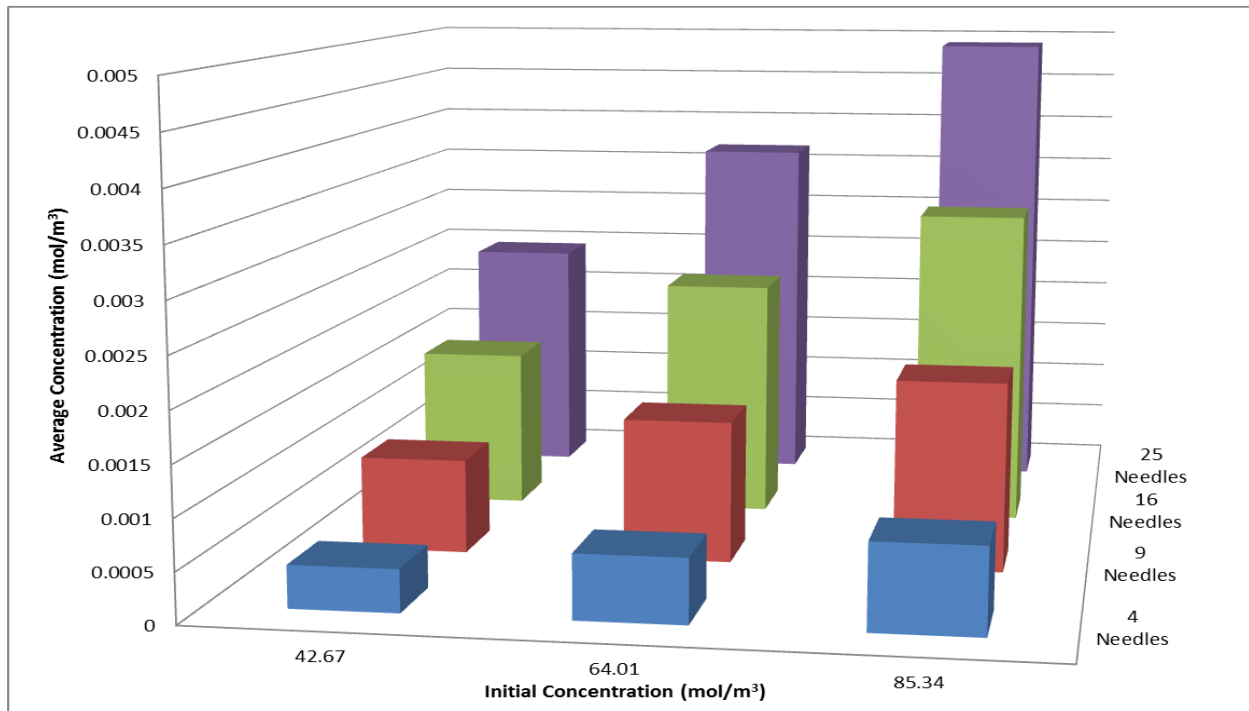


Figure 5: Optimization study of the relationship between the number of needles and the initial concentration of the anesthetic in the needles. Needle spacing was held constant at $750 \mu\text{m}$. The average concentration was taken at a $6 \text{ mm} \times 6 \text{ mm}$ square at the center of the domain at the needle-dermis interface at $t = 60 \text{ s}$. The delivered drug to this space holds a linear dependence on both initial concentration of drug and number of needles.

The study revealed that there is a linear dependence of delivered anesthetic to both the initial concentration and array size for all conditions tested. Based on these results, the optimal design for the microneedle device would contain the largest array of needles and highest initial concentration of drug, as expected.

The second optimization study conducted was to determine the relationship between the number of needles in the array and their respective spacing, the results of which are shown in Figure 6.

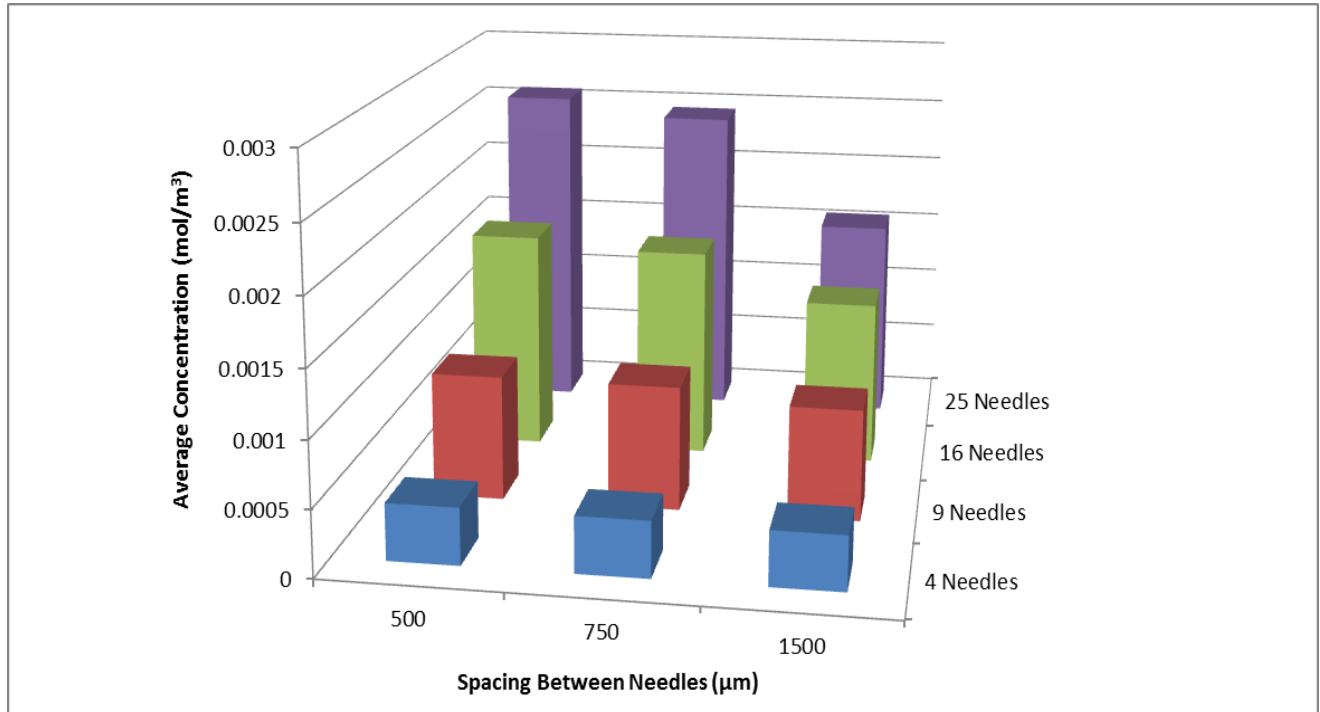


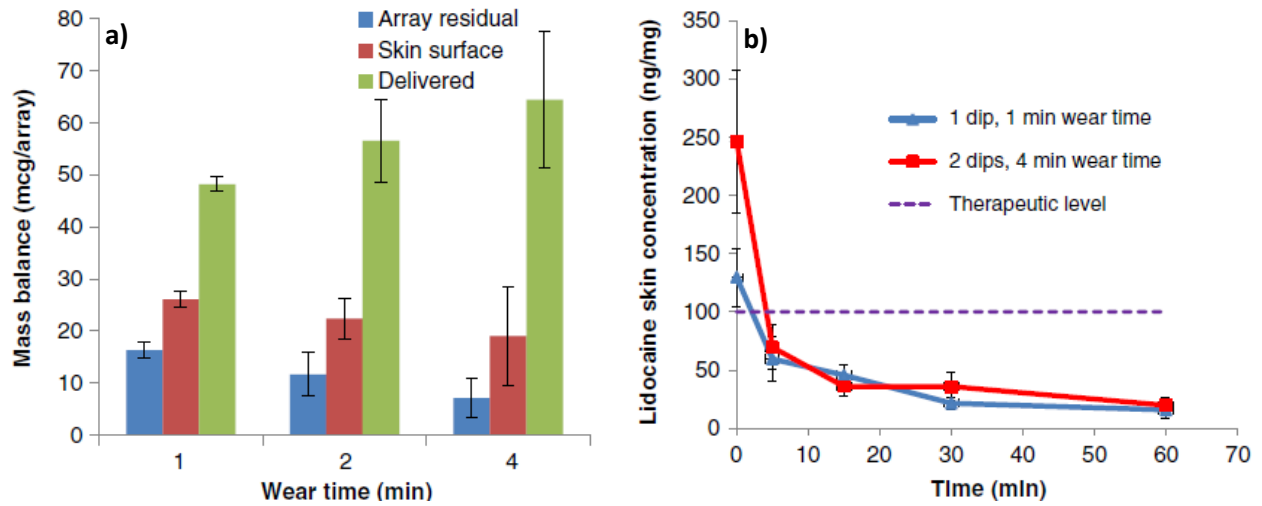
Figure 6: Optimization study of the relationship between the number of needles and spacing of the needles. Needle initial concentration was held constant at 42.67 mol/m^3 . The average concentration was taken at a $6 \text{ mm} \times 6 \text{ mm}$ square at the center of the domain at the needle-dermis interface at $t = 60 \text{ s}$. The amount of delivered drug holds a direct correlation to the number of needles, and an indirect correlation to the spacing between the needles.

The model computations revealed again that there is a direct correlation between number of needles and amount of drug delivered, but an indirect correlation between number of needles and spacing. The increased spacing of needles acted as a hindrance to the delivery of the drug by dispersing it over a larger space than the domain considered. Therefore, for targeted injection of anesthetics, reduced spacing with larger arrays of needles is optimal in this case.

Design Validation:

Once the results from the 3D solution were obtained and analyzed, the model validation by comparison to past experiments and data from literature was conducted. The concentration of lidocaine required at the nerve layer to cause anesthesia is approximately 1.0 mcg/mL , or 0.004267 mol/m^3 [10]. From Figure 5, it is apparent that for an array of 25 needles and initial concentration of 85.34 mol/m^3 , therapeutic concentration is reached for our time scale of 1 minute.

In order to validate our model, the results of our simulation were compared with experimental data of a microneedle injection as published by Zhang et. al [11]. Figure 7, taken from Zhang et. al, shows the efficiency of drug delivery from a microneedle patch with a similar array load as the model.



c)	Number of dipo	Wear time	Initial loading (mcg/array)	Delivery efficiency (%)
	1	1	90.5 ± 14.5	53.3 ± 1.6
	1	2	90.5 ± 14.5	62.4 ± 8.8
	1	4	90.5 ± 14.5	71.1 ± 1.4
	2	1	225.7 ± 13.4	16.3 ± 5.5
	2	2	225.7 ± 13.4	21.5 ± 8.8
	2	4	225.7 ± 13.4	28.3 ± 7.8

Figure 7: a) The amount of drug delivered for a microneedle array dipped in a solution of lidocaine one time (the closest to our model), across various wear times. The data for a wear time of 1 min is most relevant to the computer model. b) The lidocaine skin concentration after a patch is administered. The patch is administered for the time shown and taken off at $t = 0$ on the graph. For the patch with a 1-minute wear time, the concentration at $t = 0$ is above the therapeutic level, showing experimentally that the microneedle patch works within 1 minute. c) The amount of drug delivered for a wear time of 1 min is 48.24 mcg/array, or 0.005129 mol/m^3 .

Based on the initial loading amount and the delivery efficiency shown in Figure 7c, the amount of drug delivered in the case most similar to our model (wear time of 1 min and 1 dip) is 0.005129 mol/m^3 . This is close to our value of 0.004904 mol/m^3 from our model with an array of 25 needles and an initial concentration of 85.34 mol/m^3 , which is compared side by side in Figure 8. The number of needles used in Zhang et al.'s experiment is much higher than the 25 modeled in the computer simulation, but this is balanced by the higher initial concentration in each of our needles. This results in a similar load amount (90.5 mcg/array for the experimental data and 125.5 mcg/array for our model) and allows for an effective comparison with our model.

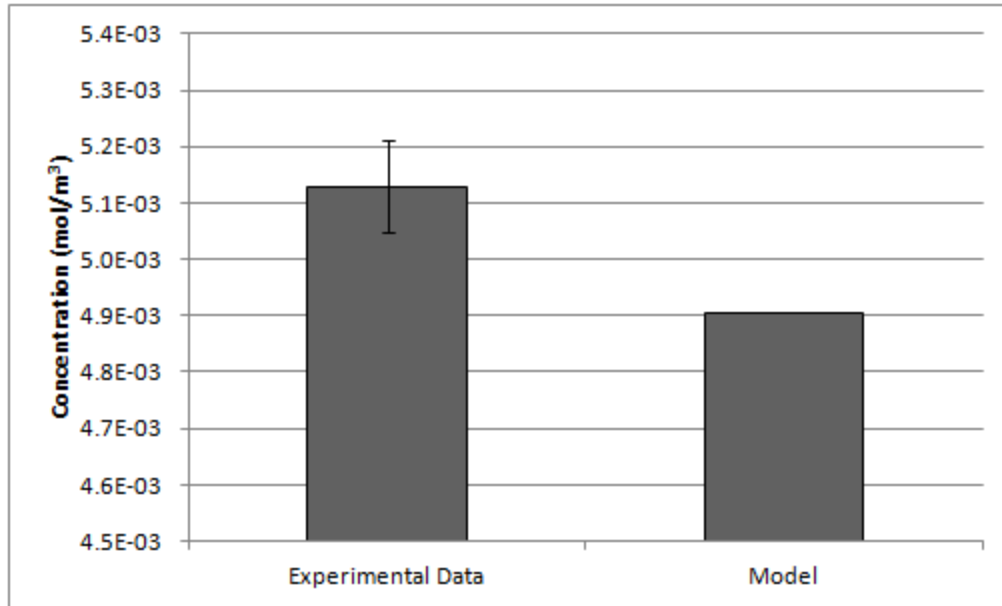


Figure 8: Experimental microneedle injection compared to model simulation. The concentration of anesthetic are similar (within an error of $0.2 \times 10^{-3} \text{ mol/m}^3$) for both the model and the experiment.

Our model is further validated by a different experiment, done by Berlin et al., which compares the efficacy of several anesthetics [12]. While this study was not conducted with microneedles, this experiment shows that lidocaine is a fast-acting anesthetic: in this study, the onset of anesthesia when lidocaine is used is about $2.2 \pm 2.7 \text{ min.}$, which is close to our model value of 1 minute. Any differences in time can be explained by the more efficient delivery method in our model.

5. Conclusion and Design Recommendations

Microneedles are painless, work as quickly as hypodermic needles, do not require any training, and do not have any foreseeable marketing problems, resulting in the recent interest for their wide-scale use. Despite their recent success in clinical trials, there still exists a need to optimize the technology for effective drug delivery. To address this issue, a computer model was developed that can be used to simulate the microneedle injection process, determine what parameters are most important in the drug delivery, and optimize the microneedle array design with respect to number of needles, spacing, and array load of anesthetic.

The model demonstrated that both the initial concentration in the microneedle and the diffusivity of the drug had a significant impact on the delivery of the lidocaine, while the permeability of the skin had a negligible effect. The primary conclusion from this data is that diffusive flux is governing the transport of the drug in the tissues. With this result, the anesthetic delivery can be enhanced by facilitating diffusion through some means, such as using an anesthetic with a higher diffusion constant, or chemically modifying the solution containing the drug to increase passive transport. In addition, increasing the initial concentration within the needles will also result in increased delivery of the drug to the tissues. However, it is important to note that both use of more drug and enhancing passive diffusion would result in a costlier treatment. In terms of array size optimization, the model demonstrated that increasing the number of microneedles increases drug delivery, also as expected. Increasing the spacing between the needles resulted in a decreased delivery of drug to the target area, due to the fact the anesthetic diffuses away from the target region below the needles. This means that microneedle patches can be optimized for targeted injection by decreasing the spacing and increasing the number of needles. Again, these modifications must be considered in the context of cost of fabrication, as well as manufacturing capabilities (in terms of resolution of needle spacing).

The ability to calculate an ideal spacing and number of needles for microneedle patches enables them to be easily and cheaply manufactured. Given that this model has successfully identified important parameters for the injection process and has been validated for use in spacing and array size optimization studies, manufacturers of this technology can utilize it to plan further clinical trial research. Ideally, these individuals could utilize the model to define critical parameters for the injection process (such as desired concentration at a certain point in the tissue, total amount of drug delivered, etc.) and vary the aspects of this model to attain the optimal performance for the specific application. This model can further be utilized to simulate injections of other substances such as vaccines, antibiotics, and other substances.

Upon successful wide-scale manufacturing of the device, the benefits of this technology over standard hypodermic needles can be enjoyed on a global scale. Painless injections will reduce the sense of anxiety and distress associated with practitioner visits. Reduction in the number of sharps injuries will limit the unintended spread of blood-borne diseases in both developed and undeveloped countries. The ease of microneedle use will also reduce the required training to inject compounds and facilitate drug delivery in field settings. Such aspects of microneedle usage will globally revolutionize the administration of local anesthetics in the medical setting.

6. Appendix A: Mathematical Statement of the Problem

Original Geometry:

Anesthetic injection was modeled in a localized section of skin. The skin was assumed to be a flat, layered domain, given that the array of microneedles is much smaller compared to the curvature of human skin as shown in Figure A1a. The microneedles were modeled to be square arrays of equally spaced cylindrical structures as in Figure A1b. The array was applied directly on the surface of the epidermis, assuming the penetration depth to be negligible.

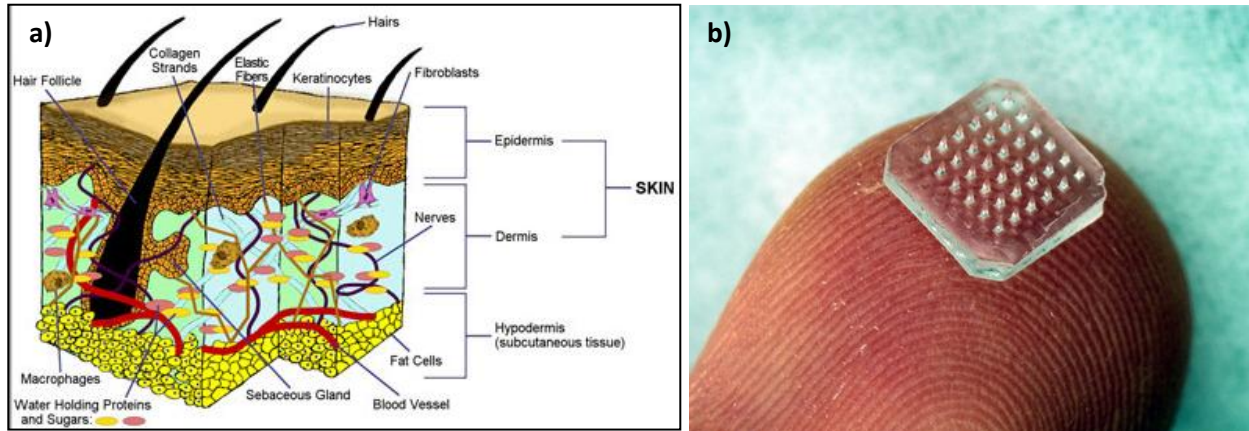


Figure A1: a) Schematic of skin layers showing the slab implemented in COMSOL. Layers that will be implemented include the epidermis, dermis, and fat layer.

(<http://reverseskinaging.com/Web%20Graphics/skinlayers.jpg>)

b) Original geometry of the microneedles showing size comparison to the skin domain. Given the small size of the microneedle array, the approximation of the skin as a slab geometry is validated.

(http://media.cleveland.com/health_impact/photo/microneedlejpg-9f75c22a29c7e323_large.jpg)

2-D Schematic

For the complete 2D solution, a 2D axisymmetric model with one microneedle was assumed. The model incorporates convection and diffusion as well as weakly compressible Navier-Stokes, which couples the Brinkman equations and Navier-Stokes fluid dynamics, to model transport of lidocaine within the skin. The schematic shown in Figure A2 was designed based on an approximation of the original skin geometry and the microneedle process as depicted by Figure A1.

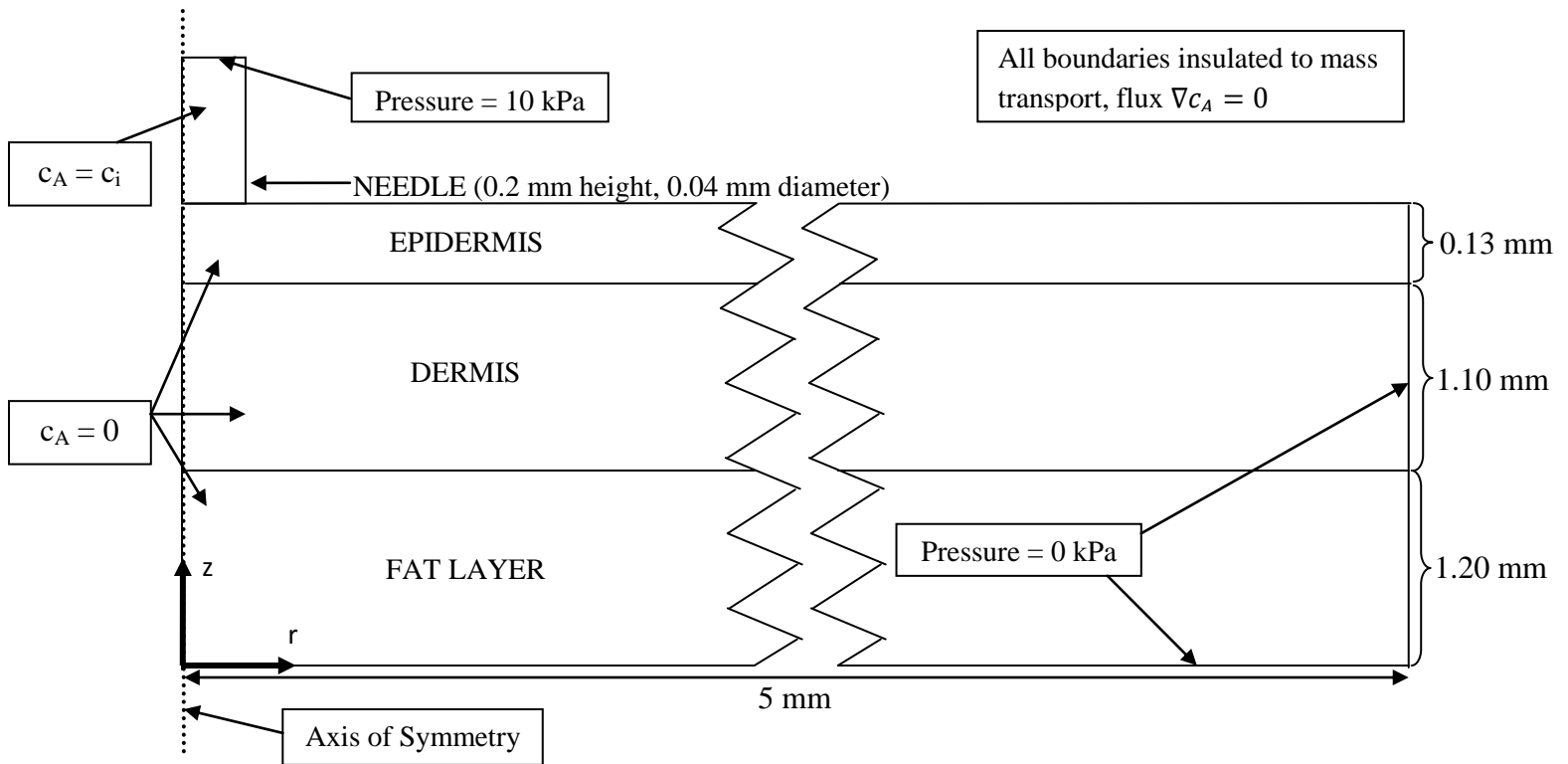


Figure A2: Schematic of the 2D COMSOL geometry showing the layers of skin. The needle is assumed to stop at the surface of the skin for easier computation. The model is axisymmetric around the z axis, incorporating one needle to model the injection process. Length and depth of the skin were set to achieve a semi-infinite boundary condition.

3-D Schematic

Based on the complex skin geometry shown in Figure A1, Figure A3 shows the simplified model consisting of all layers of skin modeled as slabs, again with cylindrical structures at the epidermis boundary to model injection of the drug. The domain dimensions were also set in order to allow the approximation of a semi-infinite boundary condition.

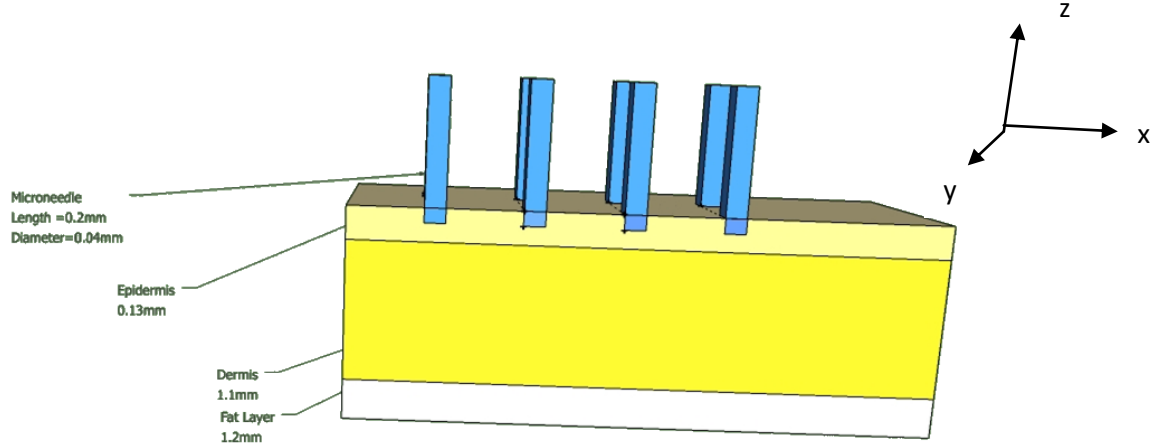


Figure A3: Microneedles and skin in a 3D model. Microneedles will be approximated as cylindrical and penetration depth will be assumed negligible. Semi-infinite boundary conditions will be implemented by creating the skin to be much larger than the microneedle array.

Governing Equations

Mass Transport:

Diffusive and convective transport of lidocaine was modeled with the vectorized temporal mass transport equation, for a model time of 60 s.

$$\frac{\partial c_A}{\partial t} + \mathbf{v} * \nabla c_A = D_A \nabla^2 c_A$$

It was assumed that due to the short time considered, there was no measurable reaction rate, and this term was dropped from the equation.

Fluid Flow:

Fluid flow was modeled in both the needle and the tissue. The needle fluid flow was assumed to follow the incompressible fluid flow form of the vectorized Navier-Stokes equations given the unobstructed flow in the needle:

$$\rho \left(\frac{\partial \mathbf{v}}{\partial t} + \mathbf{v} * \nabla \mathbf{v} \right) = -\nabla P + \mu \nabla^2 \mathbf{v}$$

The fluid flow in the tissue was assumed to be analogous to fluid flow in a porous media, thus invoking the vectorized form of the Brinkman's Flow equation. The Brinkman's equations were utilized to account for the shear stress continuity boundary condition at the needle-skin interface given the transition from incompressible to porous media flow.

$$\frac{-\mu}{k\phi} \mathbf{v} + \mu_e \nabla^2 \mathbf{v} = \nabla P$$

To account for the change in porosity of the skin with permeability, the porosity value was scaled with permeability according to their related equation.

$$k_i \propto \frac{\epsilon^3}{(1 - \epsilon)^2}$$

Boundary/Initial Conditions

Mass Transport:

The boundary conditions for the 2-D mass transport were assumed as follows:

$$\begin{aligned} c_A(r \rightarrow 5 \text{ mm}, z \rightarrow 0 \text{ mm} \} \text{ tissue}, t) &= 0 \\ \frac{\partial c_A}{\partial z} (r, z \} \text{ skin boundary, needle wall}, t) &= 0 \\ c_A(r, z \} \text{ tissue}, t = 0) &= 0 \\ c_A(r, z \} \text{ needle}, t = 0) &= c_i = 42.67 \text{ mol/m}^3 \end{aligned}$$

The needle was assumed to be impermeable to transport of drug, thus invoking the no flux condition at the needle walls. To model the semi-infinite boundary condition, the domain was created to have a very large size (Figure A5) and the concentration was set to 0 at the boundaries of the domain. At the initial time point, the concentration of anesthetic was assumed to be at 0 in the tissue and 42.67 mol/m³ [10].

The boundary conditions for the 3-D model were identical, implemented in a 3-D domain:

$$\begin{aligned} c_A(x \rightarrow \pm 2 \text{ mm}, y \rightarrow \pm 2 \text{ mm}, z \rightarrow -2.43 \text{ mm} \} \text{ tissue}, t) &= 0 \\ \frac{\partial c_A}{\partial z} (x, y, z \} \text{ skin boundary, needle wall}, t) &= 0 \\ c_A(x, y, z \} \text{ tissue}, t = 0) &= 0 \\ c_A(x, y, z \} \text{ needle}, t = 0) &= c_i = 5 \times 10^{-2} \text{ mol/m}^3 \end{aligned}$$

Fluid Flow:

The boundary conditions for the fluid flow were assumed as follows:

$$v(r \rightarrow 5 \text{ mm}, z \rightarrow 0 \text{ mm}, t) = \mathbf{0}$$

$$v(r, z \text{ } \{ \text{skin boundary, needle wall}, t) = \mathbf{0}$$

$$p(r, z \text{ } \{ \text{needle inlet}, t) = P_{\text{Applied}} = 10 \text{ kPa}$$

$$p(r, z \text{ } \{ \text{skin boundary}, t) = 0 \text{ kPa}$$

$$v(r, z \text{ } \{ \text{tissue, needle}, t = 0) = \mathbf{0}$$

The needle walls were assumed to be impermeable to the fluid flow, thus invoking the zero-velocity boundary condition at this interface. The pressure at the top of the needle was assumed to be 10 kPa [8]. As for mass transport, the domain was assumed to be semi-infinite, and this was implemented with the zero pressure and velocity conditions at the skin boundaries. At the start of the temporal model, the velocity was assumed to be zero at all points.

The boundary conditions for the 3-D model were considered identical, except implemented in a 3-D domain:

$$v(x \rightarrow \pm 5 \text{ mm}, y \rightarrow \pm 5 \text{ mm}, z \rightarrow -2.43 \text{ mm}, t) = \mathbf{0}$$

$$v(x, y, z \text{ } \{ \text{skin boundary, needle wall}, t) = \mathbf{0}$$

$$v(x, y, z \text{ } \{ \text{tissue, needle}, t = 0) = \mathbf{0}$$

$$p(x, y, z \text{ } \{ \text{needle inlet}, t) = P_{\text{Applied}}$$

$$p(x, y, z \text{ } \{ \text{tissue}, t) = 0$$

Property Values

Table A1: Property values used in the model. Values were estimated based on literature references that have developed similar models.

Convection and Diffusion	
Diffusivity Coefficient of Lidocaine, D	$1.38 \times 10^{-8} \text{ m}^2/\text{s}$ [13]
Fluid Flow	
Density of Lidocaine, ρ	999 kg/m^3 [14]
Dynamic Viscosity of Lidocaine, η	$0.001 \text{ Pa}\cdot\text{s}$ [15]
Porosity, Φ	0.5 [16]
Intrinsic Permeability of Skin, κ	10^{-17} m^2 [17]
Minimum Concentration Required at Nerves	0.004267 mol/m^3 [10]

7. Appendix B: Solution Strategy

The model development given in Appendix A was implemented with COMSOL 3.5a Multiphysics software, utilizing the convective and diffusive mass transport module to model mass transport, and the chemical engineering module for weakly compressible Navier-Stokes to model fluid flow.

Linear Solver and Space Discretization:

The linear solver for all model computation was the direct PARDISO algorithm, selectable in the COMSOL program.

Space discretization in the form of mesh was conducted similarly in both the 2-D solution and 3-D solution. The mesh was designed to account for increased accuracy required at the needle injection site while ensuring the design was computationally feasible, as given in Figure A4 for 2-D and Figure A5 for 3-D.

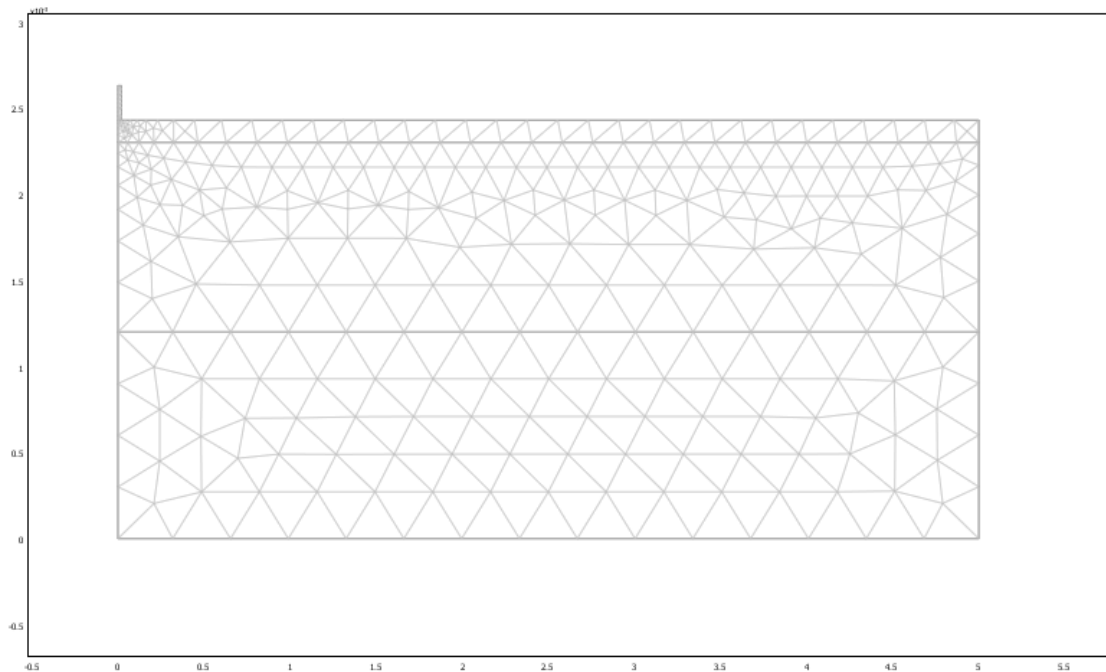


Figure A4: Schematic of meshing of COMSOL 2D model. The mesh was designed to have smaller elements at the area of the injection site, increasing to larger element size as the mesh approaches the boundary.

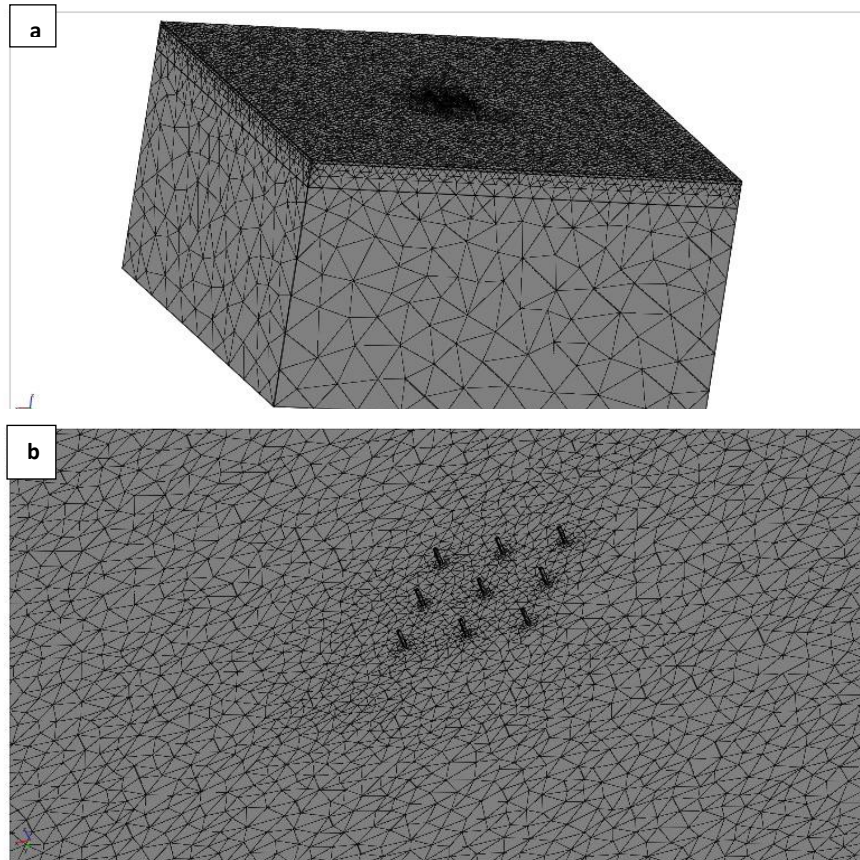


Figure A5: The mesh utilized for the 3-D solution. a) Full view of the entire domain showing the different layers of skin modeled in the mesh as well as the center area where the microneedles were positioned. b) A close-up view of the microneedles. The mesh was designed to have smaller elements near the needle that expanded in size with distance from the injection site to a maximum value.

Mesh convergence was performed by continual refining of the mesh size by shrinking each of the elements in proportion to the original scheme. The mesh convergence in the 2-dimensional model was tracked by evaluating the concentration of anesthetic at the dermis-fat layer interface directly below the needle (point $r = 0$, $z = 1.1 \times 10^{-3}$), with results shown in Figure A6.

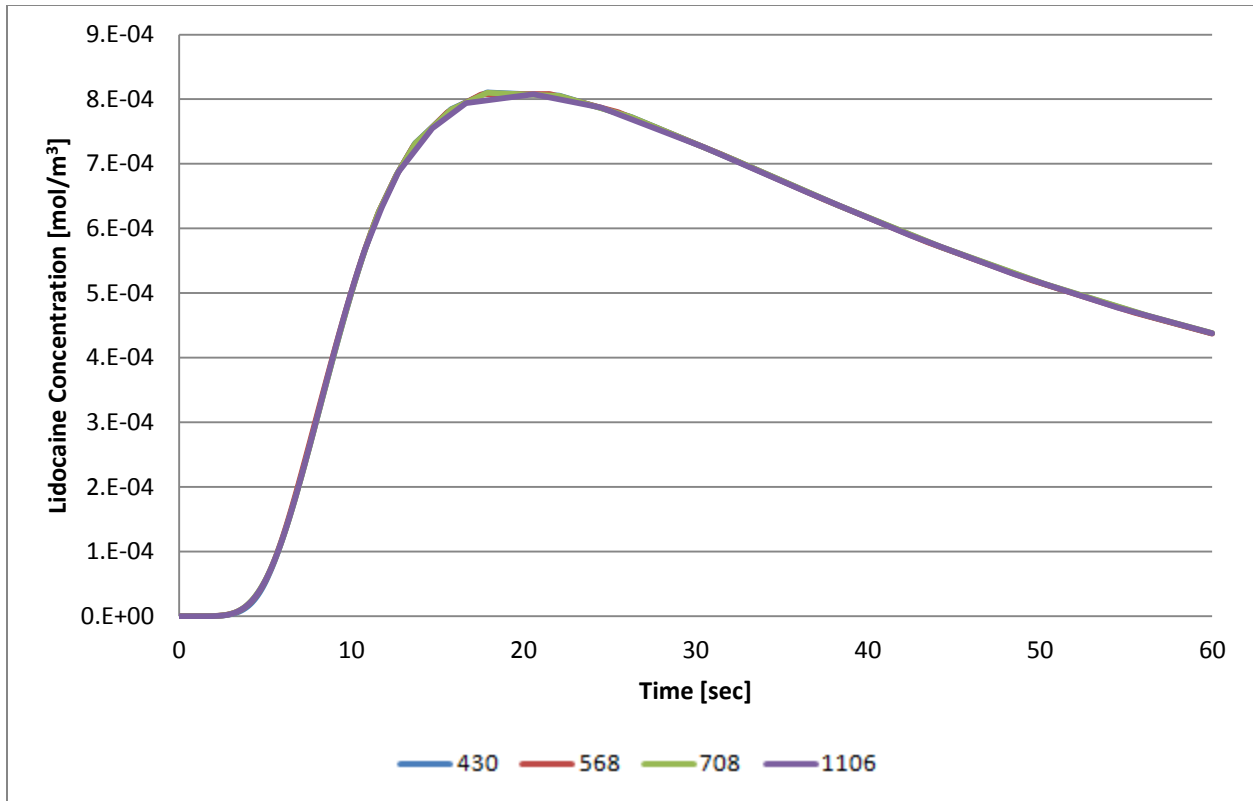


Figure A6: The concentration of lidocaine over time at point $(r, z) = (0, 1.2e-3)$ for different levels of mesh. As the plot shows, the concentration profiles converge to one particular solution as the number of finite mesh elements is increased. Since the profile remains unchanged after large increases in element size, the mesh can be considered as converged.

This point was chosen as it is representative of the area used to track the efficacy of the drug delivery, important to our design objectives. All meshes tested yielded roughly identical results, demonstrating the solution was not dependent on mesh size.

Analogous to the 2-D model, the convergence for the 3-D model was performed on the concentration of lidocaine at the point $(0.01, 0.01, 0.01)$, representing the point directly beneath the needles at the dermis-fat layer interface, the results of which are shown in Figure A7.

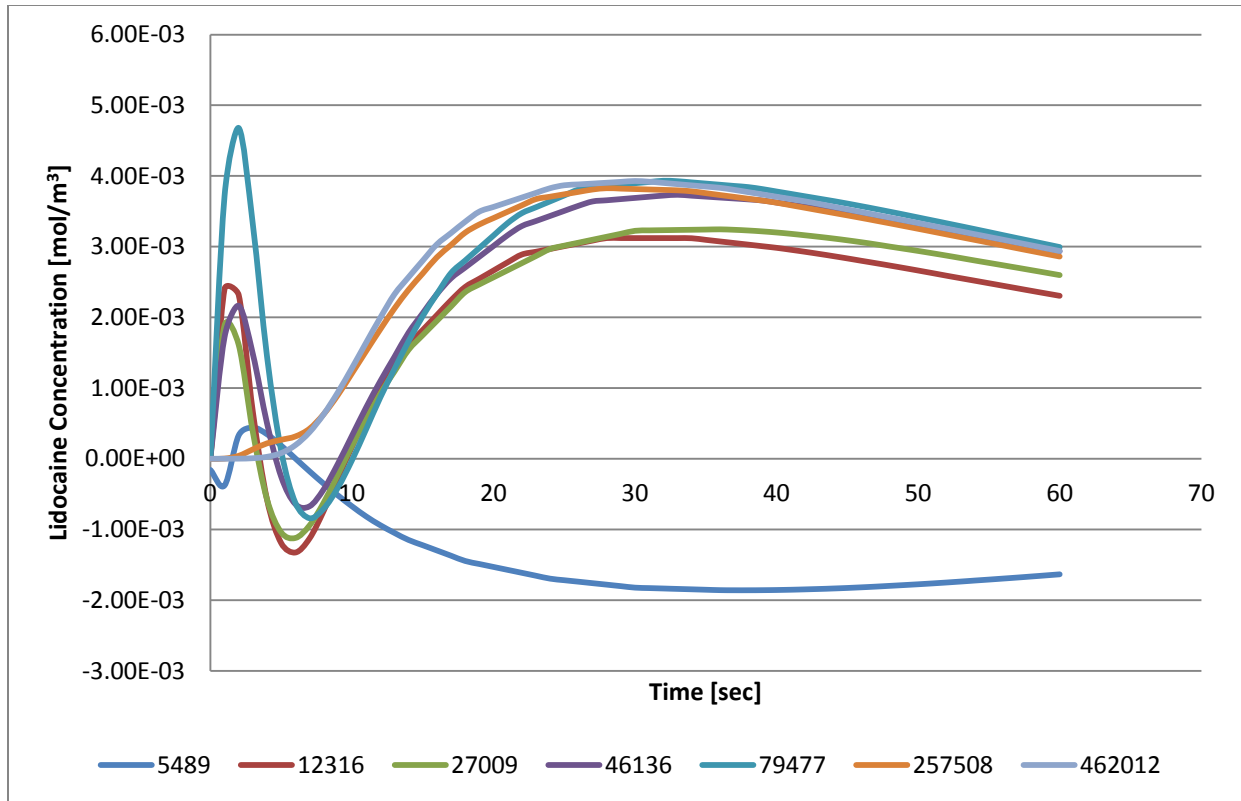


Figure A7: Mesh convergence for the model was performed for concentration of lidocaine at $(x, y, z) = (0.01, 0.01, 0.01)$, which is located at the interface between the dermis and fat layers in the center of the slab. This point approximates the location of the nerves in the skin, monitoring the efficacy of lidocaine delivery to the nerves. The mesh converged from $t = 30$ s to $t = 60$ s for coarse, normal, and fine mesh. Although there was variation for the earlier time periods, these are not considered in the analysis of how long it will take for anesthetization to occur and thus are disregarded. The numbers in the line legend represent number of elements in the mesh.

The mesh was considered to be converged at $t = 60$ s, which is the time of interest, for all meshes containing 46136 elements and above. Based on this result, the mesh with 79477 elements was utilized for 3-D model computation.

Transient Solver and Time Discretization:

The transient time stepping algorithm used was the BDF transient solver. The time step method was adaptive in that the program selected the appropriate time step based on a controlled refinement of the time step based on a recursive algorithm comparing errors between the selected time step and the previously tried time step. When the difference between the two was considered to be insignificant, the time step was considered to be converged, and the solution stored.

The absolute tolerance for the model time step computation was 0.001. This means that for all parameters computed in the model the following condition must hold (example for concentration, where i is the index of COMSOL's iterative time step estimation):

$$|c_i - c_{i-1}| < 0.001$$

The relative tolerance for the model time step computation was 0.01. This means that for all parameters computed in the model, the following condition must also hold (example for concentration, where i is the index of COMSOL's iterative time step estimation):

$$\frac{|c_i - c_{i-1}|}{c_i} < 0.01$$

Once both of these conditions were satisfied, the time step was assumed to converge.

References

- [1] Houck, C. S., & Sethna, N. F. (2005) Transdermal analgesia with local anesthetics in children: review, update and future directions. *Expert Review of Neurotherapeutics*, 5(5), 625–634.
- [2] A. Pruss-Ustun, E. Rapiti, Y. Hutin, Sharps injuries: global burden of disease from sharps injuries to health-care workers, WHO Environmental Burden of Disease Series, World Health Organization, 2003.
- [3] Kersten, G., & Hirschberg, H. (2007). Needle-free vaccine delivery. *Expert Opinion on Drug Delivery*, 4(5), 459-474.
- [4] A. Pruss-Ustun, E. Rapiti, Y. Hutin, Sharps injuries: global burden of disease from sharps injuries to health-care workers, WHO Environmental Burden of Disease Series, World Health Organization, 2003.
- [5] Gupta, J., Denson, D. D., Felner, E. I., & Prausnitz, M. R. (2012). Rapid local anesthesia in humans using minimally invasive microneedles. *Clinical Journal of Pain*, 28(2), 129-135.
- [6] Arnou, R., Icardi, G., De Decker, M., Ambrozaitis, A., & Kazek, M. P. (2009). Intradermal influenza vaccine for older adults: a randomized controlled multicenter phase III study. *Vaccine*, 27(52), 7304–7312.
- [7] Gupta, J., Felner, E. I., & Prausnitz, M. R. (2009). Minimally invasive insulin delivery in type 1 diabetic subjects using hollow microneedles. *Diabetes Technology & Therapeutics*, 11(6), 11:329–337.
- [8] Lhernould, M. S., & Delchambre, A. (2011). Innovative design of hollow polymeric microneedles for transdermal drug delivery. *Microsystem Technologies-Micro-and Nanosystems-Information Storage and Processing Systems*, 17(10-11), 1675-1682.
- [9] Stoeber, B., & Liepmann, D. (2005). Arrays of hollow out-of-plane microneedles for drug delivery. *Journal of Microelectromechanical Systems*, 14(3), 472-479.
- [10] Dorian, P., Cass, D., Schwartz, B., Cooper, R., Gelaznikas, R., & Barr, A. (2002). Amiodarone as compared with lidocaine for shock-resistant ventricular fibrillation. *The New England Journal of Medicine*, 346(12), 884-890.
- [11] Zhang, Y., Brown, K., Siebenaler, K., Determan, A., Dohmeier, D., & Hansen, K. (2012). Development of Lidocaine-Coated Microneedle Product for Rapid, Safe, and Prolonged Local Analgesic Action. *Pharmaceutical Research*, 29(1), 170-177.
- [12] Berlin, J., Nusstein, J., Reader, A., Beck, M., & Weaver, J. (2005). Efficacy of articaine and lidocaine in a primary intraligamentary injection administered with a computer-controlled

- local anesthetic delivery system. *Oral Surgery, Oral Medicine, Oral Pathology, Oral Radiology, and Endodontics*, 99(3), 361-366.
- [13] Pjanovic, R., Boskovic-Vragolovic, N., Veljkovic-Giga, J., Garic-Grulovic, R., Pejanovic, S., & Bugarski, B. (2010). Diffusion of drugs from hydrogels and liposomes as drug carriers. *Journal of Chemical Technology and Biotechnology*, 85(5), 693-698.
- [14] Hare, G. M. T., & Ngan, J. C. S. (1998). Density determination of local anaesthetic opioid mixtures for spinal anaesthesia. *Canadian Journal of Anaesthesia*, 45(4), 341-346.
- [15] Anderson, J. L., Tucker, E. M., Pasyk, S., Patterson, E., Simon, A. B., Burmeister, W. E., Lucchesi, B. R., & Pitt, B. (1982). Long-term intravenous infusion of antiarrhythmic drugs using a totally implanted drug delivery system. *The American Journal of Cardiology*, 49(8), 1954-1958.
- [16] Choi, Y. S., Hong, S. R., Lee, Y. M., Song, K. W., Park, M. H., & Nam, Y. S. (1999). Studies on gelatin-containing artificial skin: II. Preparation and characterization of cross-linked gelatin-hyaluronate sponge. *Journal of Biomedical Materials Research*, 48(5), 631-639.
- [17] Datta, A. K. (2006). Hydraulic Permeability of Food Tissues. *International Journal of Food Properties*, 9(4), 767-780.